archives
of thermodynamics
Vol. **42**(2021), No. 2, 121–153
DOI: 10.24425/ather.2021.137557

Numerical modeling of heat transfer in Al_2O_3/H_2O nanofluid flowing through a Bessel-like converging pipe

CHUKWUKA S. IWEKA[a]*
OLATOMIDE G. FADODUN[b]

[a] Department of Mechanical Engineering, Delta State Polytechnic, Ozoro, P.M.B 5, Ozoro 334111, Delta State, Nigeria

[b] Centre for Energy Research and Development, Obafemi Awolowo University, Ile-Ife 220282, Osun State, Nigeria

Abstract This paper studies hydrodynamic and heat transfer performance of Al_2O_3/H_2O nanofluid flowing through a Bessel-like converging pipe in laminar flow regime using the computational fluid dynamic approach. A parametric study was carried out on the effect of Reynolds number (300–1200), convergence index (0-3) and nanoparticle concentration (0–3%) on the both hydrodynamic and thermal fields. The results showed the pressure drop profile along the axial length of the converging pipes is parabolic compared to the downward straight profile obtained in a straight pipe. Furthermore, an increase in convergence index, Reynolds number and nanoparticle concentration were found to enhance convective heat transfer performance. Also, a new empirical model was developed to estimates the average Nusselt number as a function of aforementioned variables. Finally, the result of the thermohydraulic performance evaluation criterion showed that the usage of Bessel-like converging pipes is advantageous at a low Reynolds number.

Keywords: Nanofluid, Nusselt number; Response surface methodology; Reynolds number; Convergence index

*Corresponding Author. Email: chukwuka.iweka@dspz.edu.ng

Nomenclature

c	–	specific heat of water, kJ/kg$^\circ$C
C_f	–	skin friction coefficient
C_p	–	specific heat capacity at constant pressure, J/kgK
D_h	–	diameter of the pipe, m
d_f	–	diameter of water molecule, nm
d_P	–	diameter of nanoparticle, nm
dP	–	local pressure drop, Pa
f	–	friction factor
h	–	heat transfer coefficient
M	–	molecular mass of water, kg/mol
Nu	–	Nusselt number
n	–	convergence index, normal to the wall surface
K_b	–	Boltzmann constant J/K
Pr	–	Prandtl number of base fluid
$(\mathrm{PEC})_{\mathrm{geo}}$	–	geometry performance evaluation criterion
$(\mathrm{PEC})_{\mathrm{nano}}$	–	nanofluid performance evaluation criterion
q''	–	heat flux at the surface of the pipe, W/m^2
P	–	pressure, Pa
R^2	–	coefficient of determination
Re	–	nanoparticle Reynolds number
r	–	radial distance, m
T	–	temperature, K
T_{in}	–	inlet temperature of base fluid, K
u	–	velocity, m/s
u_r, u_x	–	components velocity, m/s
x	–	axial distance, m

Greek symbols

λ	–	thermal conductivity, W/m K
μ	–	dynamic viscosity, kg/m·s
ρ	–	density of base fluid, kg/m^3
φ	–	nanoparticle volume fraction, %

Subscripts

ave	–	average
bf	–	base fluid
f	–	base fluid at inlet
fr	–	freezing point
in	–	inlet
out	–	outlet
p	–	nanoparticle
np	–	nanoparticle
s	–	wall

Abbreviations

RSM	–	response surface methodology

1 Introduction

The augmentation of convective heat transfer has continued to receive a lot of attention from researchers because of the big role it plays in the optimization of thermal designs. Generally, techniques for enhancing convective heat transfer can broadly be classified into three groups: active techniques which include the usage of an active device powered by a mechanical device or electrostatic filed, passive techniques which consist of geometry modifications or enhancement of thermophysical properties of coolant to enhance convective heat transfer, while the third category are combined active and passive techniques. The literature survey showed that the passive technique is more preferable compared to the active technique because it requires no external power to facilitate the enhancement of convective heat transfer. Various geometry modifications have been studied by researchers so far, among those considered, converging pipe is one of the most preferable because the enhancement of convective heat transfer is accompanied by a lower pressure drop compared to other designs [1–7].

There are limited works on heat transfer performance of nanofluid flowing through a converging pipe in the literature. Among the few ones is the work of Al-Sammarraie *et al.* [8], where the authors investigated the effect of convergence angle (0°–25°) and Reynolds number on the hydrodynamic and heat transfer performance of nanofluid flowing through a converging pipe in a laminar flow regime. The authors reported that an increase in convergence angle enhances convective heat transfer. In another work, Al-Sammarraie *et al.* [9] investigated the heat transfer performance of Al_2O_3–water nanofluid flowing through concave and convex pipes. The author claimed that the concave pipe has higher heat transfer performance than convex pipe, while the convex pipe has higher the thermohydraulic performance factor than concave pipe.

Some researchers have studied heat transfer performance in fluid flowing through pipes with geometry different from that of converging pipes. Examples of these include the work of Davood *et al.* [10], where the authors studied the convective heat transfer performance of nanofluid flowing through a wavy channel. The authors claimed that an increase in wavelength enhances the convective heat transfer performance. Xie *et al.* [11] investigated convective heat transfer performance of nanofluid flowing through the dimple and protrusion channels. The authors reported that the dimple channel enhances convective heat transfer better than the protrusion channel. Anvari *et al.* [12] examined the effect of channel waviness and nanoparticle concentration on heat transfer performance of carboxyl-methyl cellulose-water

nanofluid. The authors concluded that an increase in waviness and nanoparticle concentration enhances the heat transfer performance and pressure drop. Salman investigated nanofluid heat transfer performance in trapezoidal, triangular, and rectangular ribs [13]. The author reported that the three ribs enhance convective heat transfer. Furthermore, among the three ribs considered, the triangular rib exhibited the highest heat transfer performance. Huminic and Huminic considered the effect of geometry on heat transfer performance of hybrid nanofluid flow through a channel with different cross-sections [14]. The authors claimed that a square duct has higher heat transfer performance compared to a circular duct. Pourfattah *et al.* [15] investigated the heat transfer performance of nanofluid flowing through a channel. The authors considered the effect of the dimple on the channel wall and reported enhancement in convective heat transfer performance. Khoshvaght examined the heat transfer performance of nanofluid flow through a wavy channel [16]. The author claimed that the heat transfer performance in a wavy channel is higher compared with a smooth channel. Rashidi *et al.* [17] investigated the convective heat transfer performance of nanofluid flowing through a wavy channel. The effect of channel waviness and corrugation height on hydrodynamic and heat transfer performance was considered. The authors claimed that an increase in corrugated height enhances the convective heat transfer performance. Manca *et al.* [18] studied the mixed convective heat transfer performance of Al_2O_3–water nanofluid through a triangular duct. Finally, Ahmed *et al.* [19], investigated the forced convective heat transfer performance of Al_2O_3–water nanofluid flowing through a triangular corrugation channel.

Experimental design plays an important role in science and engineering as it avails us of the opportunity to determine the influence of independent variables on the dependent variables. One of the popular experimental designs for process optimization is response surface methodology (RSM). This technique shows the effect of input variables and the interaction between the input variables on the output variable [20,21]. Fadodun *et al.* [22] developed an empirical model for Nusselt number and pressure drop of nanofluid flowing through a pipe in turbulent flow regime using RSM. The work focused on the effect of four independent variables (inlet temperature, Reynolds number, nanoparticle concentration, and nanoparticle size) on average Nusselt number and pressure drop. In another work, Fadodun *et al.* [23] developed an empirical model to estimate the irreversibility production rate of Al_2O_3 nanofluid fluid flowing through a pipe as a function of four independent variables (inlet temperature, Reynolds number, nanoparticle concentration, and nanoparticle size) using RSM. Shirvan *et al.* [24]

employed RSM to develop an empirical correlation that estimates the average Nusselt number of nanofluid flowing through a pipe in laminar flow. The result of the sensitivity analysis performed on the empirical model showed that the Reynolds number has positive sensitivity on the average Nusselt number while nanoparticle size has negative sensitivity. Fadodun *et al.* [25] used RSM to obtain a new correlation that estimates irreversibility production rate of Al_2O_3 nanofluid flowing through a converging pipe of various angles. Chan *et al.* [26] developed an empirical model for the average Nusselt number of nanofluid flowing in a pipe using RSM. The work considered the effect of inlet velocity and inlet temperature on heat transfer performance. Finally, Nookaraju used RSM to developed an empirical model for the average Nusselt number of nanofluid flowing in a helical groove pipe. The effect of concentration and twist ratio on the average Nusselt number were examined [27].

From the review of literature, there are limited works on the hydrodynamic and heat transfer performances of nanofluid flowing through converging pipes. The available ones only considered linear converging pipes. Furthermore, to the best of our knowledge, no work has used RSM to estimate the heat transfer performance of nanofluids flowing through a converging pipe. Therefore, this study aimed at: (i) examination of the convective heat transfer performance of nanofluid flowing through a Bessel-like converging pipe in the laminar flow regime; (ii) investigation of the effect of Reynolds number $300 \leq \mathrm{Re} \leq 1200$, nanoparticle concentration $0\% \leq \varphi \leq 3\%$, and convergence index $0 \leq n \leq 3$ on hydrodynamic and heat transfer performance of Al_2O_3/H_2O nanofluid flowing through Bessel-like converging pipes using the computational fluid dynamic approach; (iii) development of an empirical model using RSM to estimate the average Nusselt number of Al_2O_3/H_2O nanofluid in Bessel-like converging pipes as a function of the three aforementioned variables. In the further present is variation in temperature, Nusselt number, friction factor, velocity contour, and pressure drop as a function of Reynolds number, convergence index, and nanoparticle concentration. Furthermore, sensitivity analysis on the empirical model developed is presented.

2 Methodology

Considered laminar forced convective heat transfer in Al_2O_3/H_2O nanofluid flowing through a converging pipe whose cross-section along the axial direction varies in Bessel manner as shown in Fig. 1. The dimension and ge-

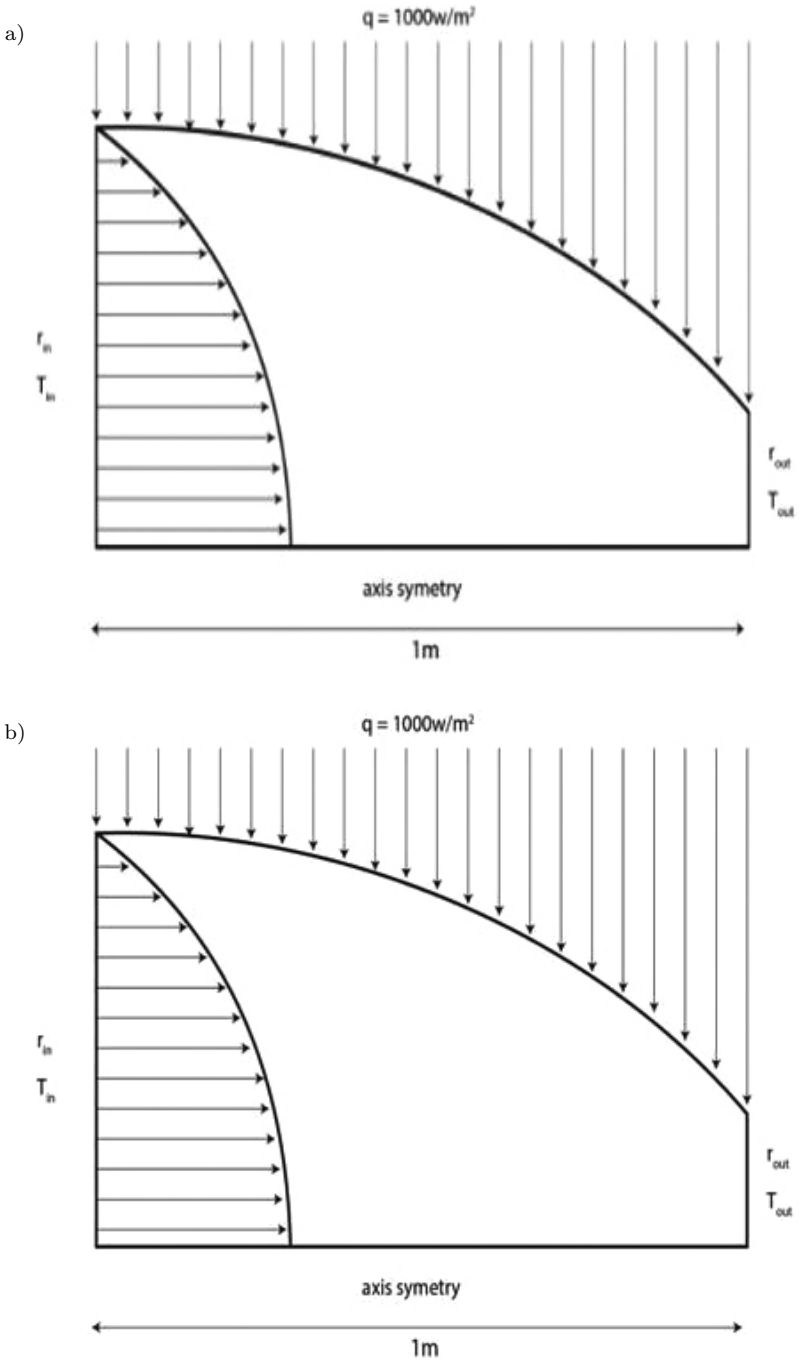

Figure 1: a), b). For legend see nextpage.

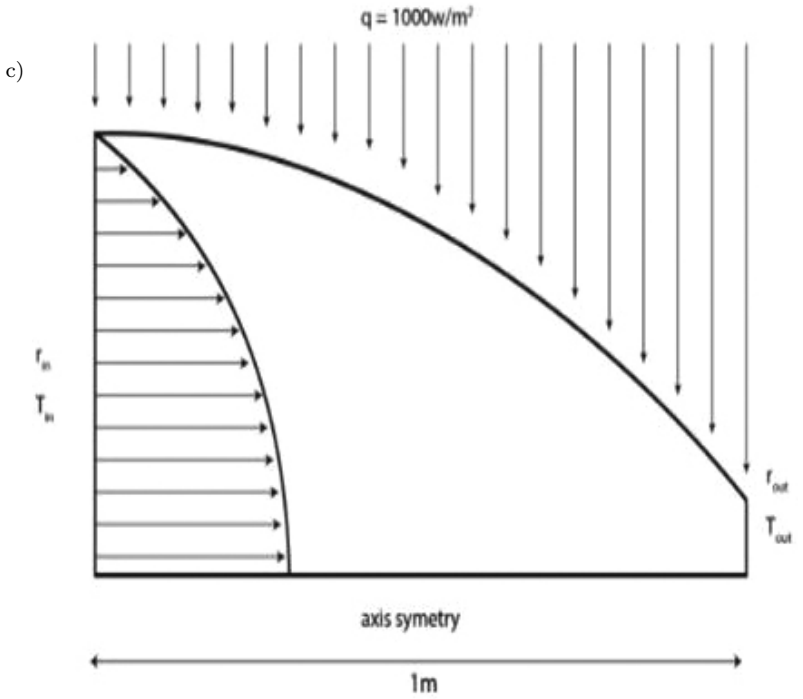

Figure 1: Schematic diagram of the problem: a) $r(x) = r_{in}(J_0(x))^1$, b) $r(x) = r_{in}(J_0(x))^2$, c) $r(x) = r_{in}(J_0(x))^3$.

ometry of the pipes are presented in Table 1. Also, the flow is assumed to be fully developed at the inlet section and a constant heat flux of 1000 W/m^2 was applied to the surface wall of the pipe. Furthermore, both flow and thermal fields were assumed to be symmetric about the axial coordinate.

Table 1: Geometric dimension of the convergent pipe of 1 m length.

Radius of pipe inlet, r_{in}	Convergence index, n	Radius of pipe outlet, $r_{out}(x) = r_{in}(J_0(x_{out}))^n$ (m)	Label
0.05	0	0.05000	H0
0.05	1	0.03826	H1
0.05	2	0.029276	H2
0.05	3	0.02240	H3

In this work the following assumptions were made:

- flow of nanofluid inside the duct is laminar, steady-state and 2D ax-

isymmetric;

- nanoparticle dispersed in the base fluid is fluidized and the resulting suspension can be treated as a single-phase model;
- both nanoparticle and base fluid are in thermal equilibrium and there is no-slip between them;
- nanofluid is assumed to be incompressible and thermophysical are maintained constant;
- radiation and viscous dissipation are negligible.

2.1 Governing equations

The governing (continuity, momentum, and energy) are expressed as [28]:

$$\frac{\partial u_r}{\partial r} + \frac{\partial u_x}{\partial x} + \frac{u_r}{r} = 0\,, \tag{1}$$

$$\rho\left(u_r\frac{\partial u_x}{\partial r}+u_x\frac{\partial u_x}{\partial x}\right) = -\frac{\partial P}{\partial x}+\left[\frac{\mu}{r}\frac{\partial u_x}{\partial r}+\mu\left(\frac{\partial^2 u_x}{\partial r^2}+\frac{\partial^2 u_x}{\partial x^2}\right)\right], \tag{2a}$$

$$\rho\left(u_r\frac{\partial u_r}{\partial r}+u_x\frac{\partial u_r}{\partial x}\right) = -\frac{\partial P}{\partial r}+\left[-\frac{\mu}{r}\frac{u_r}{r}+\frac{\mu}{r}\frac{\partial u_r}{\partial r}+\mu\left(\frac{\partial^2 u_r}{\partial r^2}+\frac{\partial^2 u_r}{\partial x^2}\right)\right], \tag{2b}$$

$$\rho C_p\left(u_r\frac{\partial T}{\partial r}+u_x\frac{\partial T}{\partial x}\right) = \frac{\lambda}{r}\frac{\partial T}{\partial r}+\lambda\left(\frac{\partial^2 T}{\partial r^2}+\frac{\partial^2 T}{\partial x^2}\right). \tag{3}$$

The local pipe radius is expressed as

$$r(x) = r_{in}\left(J_0(x)\right)^n, \tag{4}$$

where J_0 is the Bessel functions of the first kind of order, r_{in} is the radius of pipe inlet, and $n = 0, 1, 2, 3$ is the convergence index.

2.2 Boundary conditions

The following boundary conditions are prescribed:

- inlet section: $u_x = u_{in}\left[1-\left(\frac{y}{R}\right)^2\right]$, $\quad u_r = 0\,,\quad T_{in} = 300$ K;
- outlet section: $\frac{\partial u_r}{\partial x} = 0\,,\quad \frac{\partial u_x}{\partial x} = 0\,,\quad \frac{\partial T}{\partial x} = 0\,,\quad P_{\text{gauge}} = 0$ Pa;

- wall: $u_x = 0\,, \quad u_r = 0\,, \quad T_s = T_f - \lambda_s \dfrac{\partial T_s}{\partial n} = -\lambda_f \dfrac{\partial T_f}{\partial n}\,, \quad q'' = 1000 \dfrac{\mathrm{W}}{\mathrm{m}^2}$;
- symmetry line: $\dfrac{\partial u_r}{\partial r} = 0\,, \quad \lambda \dfrac{\partial T}{\partial r} = 0\,.$

2.3 Thermophysical properties of water

Thermophysical properties of water (density, viscosity, specific capacity and thermal conductivity) as functions of temperature are given as [29]:

$$\rho_f = 330.12 + 5.92T - 1.63 \times 10^{-2}T^2 + 1.33 \times 10^{-5}T^{-3}\,, \tag{5}$$

$$C_p = 10^{-3}\left(10.01 - 5.14 \times 10^{-2}T + 1.49{\times}10^{-4}T^2 - 1.43{\times}10^{-7}T^3\right), \tag{6}$$

$$\mu_f = 0.00002414 \times 10^{\left(\frac{247.81}{T-140}\right)}, \tag{7}$$

$$k_f = 0.76761 + 7.53211 \times 10^{-3}T - 0.98244 \times 10^{-5}T^2. \tag{8}$$

2.4 Single-phase model

The thermophysical properties of nanofluid $(\rho_{nf}, C_{nf}, \mu_{nf}, \lambda_{nf})$ are modeled using a single phase-model expressed as [30–32]:

$$\rho_{nf} = (1-\varphi)\rho_{bf} + \varphi\rho_{np}\,, \tag{9}$$

$$C_{nf} = \frac{(1-\varphi)\,(\rho C_p)_{bf} + \varphi\,(\rho C_p)_{np}}{\rho_{nf}}\,, \tag{10}$$

$$\frac{\mu_f}{\mu_{nf}} = 1 - 34.87\left(\frac{d_p}{d_f}\right)^{-0.3}\varphi^{1.03}\,, \tag{11}$$

$$\frac{\lambda_{nf}}{\lambda_f} = 1 + 4.4\mathrm{Re}_p^{0.4}\mathrm{Pr}_f^{0.66}\left(\frac{T_{nf}}{T_{fr}}\right)^{10}\left(\frac{k_{np}}{k_f}\right)^{0.33}\varphi^{0.66}\,, \tag{12}$$

where T_{fr} is the freezing point of the base fluid. The thermophysical properties of Al_2O_3 and water are shown in Table 2.

Table 2: Properties of Al_2O_3 [23].

Material	Parameters			
	C_p (J/K)	ρ (kg/m^3)	λ (W/mK)	M
Al_2O_3	765	3970	42	
H_2O	4200	1000	0.609	0.00085

2.5 Hydrodynamics and heat transfer

The inlet velocity calculated from the prescribed Reynolds number is expressed as

$$u_{in} = \frac{\mathrm{Re}\mu_{nf}}{\rho D_h}\,. \tag{13}$$

The friction factor and local friction factor are expressed in the form [33,34]:

$$f = \frac{2D_h\Delta p}{\rho u^2 L}\,, \tag{14}$$

$$C_f = \frac{2\tau_w}{\rho u^2}\,, \tag{15}$$

where Δp is the pressure drop, u is the velocity, and L is the channel length, and τ_w is the wall shear stress.

The heat transfer coefficient is calculated as

$$h(x) = \frac{q''}{T_s(x) - T_f(x)}\,, \tag{16}$$

where

$$T_f(x) = \frac{\int\limits_0^{r(x)} u_x(r)T(r)r\,\mathrm{d}r}{\int\limits_0^{r(x)} u_x(r)r\,\mathrm{d}r}\,. \tag{17}$$

The average heat transfer coefficient is evaluated as [28]

$$h_{\mathrm{ave}} = \frac{1}{L}\int\limits_0^L h(x)\,\mathrm{d}x. \tag{18}$$

The average Nusselt number is given as

$$\mathrm{Nu}_{\mathrm{ave}} = \frac{h_{\mathrm{ave}}D_h}{k}\,. \tag{19}$$

The correlation for the local Nusselt number in straight pipes as proposed by Shah-London is given as [35]

$$\mathrm{Nu}_z = \frac{hD_h}{k} = \begin{cases} 1.077Z^{*-1/3} - 07 & \text{for} \quad Z^* \le 0.01, \\ 3.657{+}6.874\left(10^3 Z^*\right)^{-0.488} e^{-57.2Z^*} & \text{for} \quad Z^* \ge 0.01, \end{cases} \tag{20}$$

where $Z^* = \dfrac{\dfrac{x}{D_h}}{\mathrm{RePr}}$.

The geometry performance evaluation criterion $(\mathrm{PEC})_{\mathrm{geo}}$ is defined as

$$(\mathrm{PEC})_{\mathrm{geo}} = \frac{\dfrac{\mathrm{Nu}_{\mathrm{converging}}}{\mathrm{Nu}_{\mathrm{stright}}}}{\left(\dfrac{f_{\mathrm{converging}}}{f_{\mathrm{stright}}}\right)^{0.33}} . \tag{21}$$

Likewise, the nanofluid performance evaluation criterion $(\mathrm{PEC})_{\mathrm{nano}}$ is defined as

$$(\mathrm{PEC})_{\mathrm{nano}} = \frac{\dfrac{\mathrm{Nu}_{\mathrm{nanofluid}}}{\mathrm{Nu}_{\mathrm{water}}}}{\left(\dfrac{f_{\mathrm{nanofluid}}}{f_{\mathrm{water}}}\right)^{0.33}} . \tag{22}$$

2.6 Response surface methodology

The response surface methodology (RSM) is performed using the central composite method, the input variables are Reynolds number, convergence index, and nanoparticle concentration, and the output variable is the average Nusselt number. Each input variable is divided into three levels ($k = 3$) and condition of 20 runs is defined as $(2^k + 2k + 6)$. This consists of 14 non-center points and 6 center points [36]. Table 3 shows the value associated with each level of the independent variables. The RSM was carried out using Design-Expert software [37].

Table 3: Variables and the value associated with level used in RSM.

Variable	Level		
	–1	0	1
Reynolds number	600	900	1200
Convergence index	1	2	3
Volume ratio (%)	1	2	3

3 Numerical solution and verification

The entire domain was discretized using a structured four-node element mesh as shown in Fig. 2. Small size elements were used near the wall to capture the rapid change in the field variables at the boundary layer [38,39].

a)

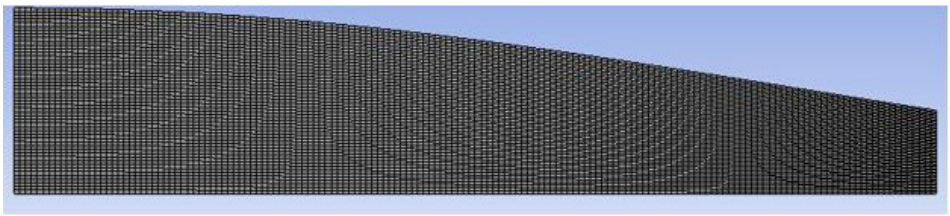

b)

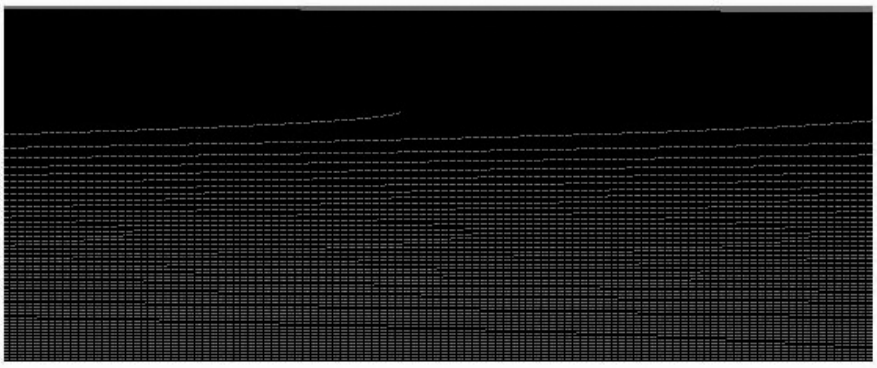

Figure 2: a) Structure of the mesh grid. b) Enlarge mesh profile showing small mesh size near the wall.

The governing equations expressed in Eq. (1)–(3) and boundary condition presented in Sec. 2.2 were solved using a pressure-based finite-volume method in Ansys Fluent 19.2 [40]. Here, the governing equations were integrated over each control volume to obtain algebraic equations for velocity and the temperature fields (u_x, u_r, T). The pressure equation is derived from momentum and continuity equations such that the velocity field corrected by the pressure satisfies the equation of continuity. Here, the semi-implicit pressure linked equation (SIMPLE) algorithm was used for pressure-velocity coupling [23]. The resulting algebraic equations were solved iteratively to obtain the updated solution. The convergence criteria for the iteration were set to 10^{-6} (the residual of continuity, momentum and energy equation is less than 10^{-6}, that is

$$\left| \frac{\Gamma^{i+1} - \Gamma^{i}}{\Gamma^{i+1}} \right| \leq 10^{-6}\,, \tag{23}$$

where the superscript i represents the iteration number and Γ represents field variables. The grid refinement was performed by varying the number of mesh elements used to estimate the average Nusselt number of 1.6% Al_2O_3/H_2O nanofluid flowing through a straight pipe at the Reynolds number of 1650. The result was compared with the experimental value of Wen and Ding where the average Nusselt number of Al_2O_3/H_2O nanofluid flowing through a copper tube in a laminar flow regime was calculated [41]. The experimental system consists of a flow loop made of a cooper tube of length 0.97 m and inner diameter 0.0045 m heated by a flexible rubber heater of rated power 300 W. Five T-type thermocouples were mounted on the tube surface along the axial direction while another two thermocouples were inserted into the tube at the entry and exit sections to measure the bulk temperature. The comparison of the two results is shown in Table 4.

Table 4: Present result with experimental result of Wen and Ding [36] at Re = 1650 for 1.6% Al_2O_3/H_2O nanofluid.

Grids ($N_r \times N_x$)	Present study	Experimental: Wen and Ding [35]	Error (%)
50×500	8.40	9.7	13.40
80×800	8.96	9.7	7.63
100×700	9.24	9.7	4.74
150×750	9.36	9.7	3.51
150×850	9.38	9.7	3.30

Several combinations were tested until the optimum configuration ($N_r = 150$, $N_x = 850$, where N_r and N_x are the number of nodes in radial and longitudinal directions, respectively), was achieved, and further increase in the number of grid elements did not change the value of the average Nusselt number more than 3%. To further ascertain the accuracy of the mesh configuration, the local variation of Nusselt number of distilled H_2O along the axial distance of the pipe at the Reynolds number of 10^3 was estimated and the result was compared with Shah and London correlation expressed by Eq. (20). The comparisons of the two results are shown in Fig. 3. Also, the local heat transfer coefficient, $h(x)$, for 1.6% Al_2O_3/H_2O nanofluid was estimated and compared with the experimental result of Wen and Ding [41]. The comparison is shown in Fig. 4. Furthermore, the variation of the average Nusselt number of 2% Al_2O_3/H_2O nanofluid against the Peclect number was estimated and compared with the experimental result of Heris *et al.* [42] where the average Nusselt number of 2% Al_2O_3/H_2O nanofluid

flowing through a circular pipe under constant wall temperature in laminar flow regime was estimated. The experimental setup consists of a flow loop made of an annular cooper tube of length 1 m, thickness 0.0005 m and diameter 0.032 mm. K-type thermocouples of precision 0.1 K were welded on the tube surface by 0.1 m apart. Another two K-type thermocouples were

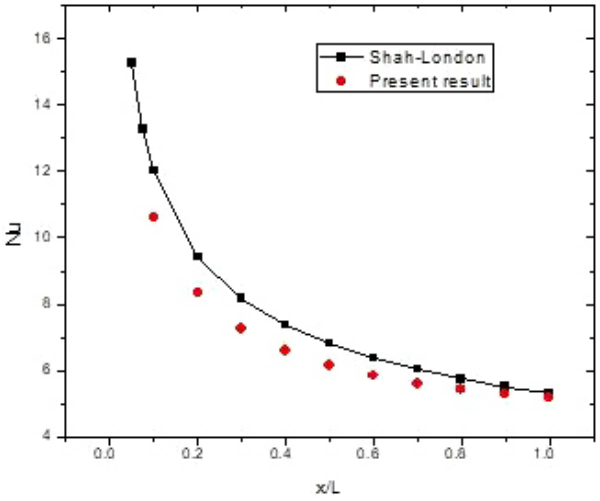

Figure 3: Comparison of local Nusselt number with Shah and London equation at Re = 1000.

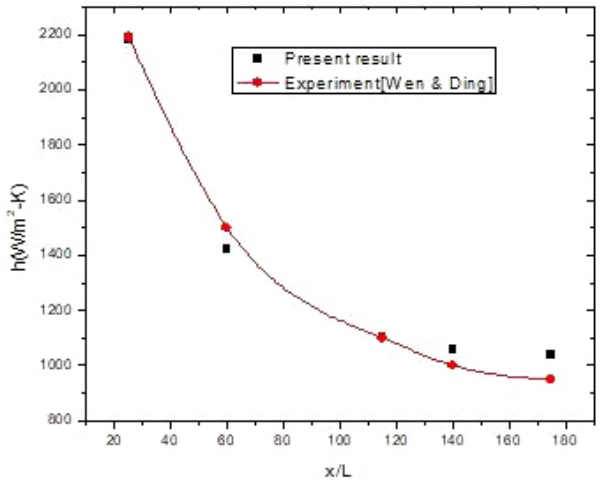

Figure 4: Comparison of local heat transfer coefficient with experimental data of Wen and Ding [35] at Re = 1000.

inserted into entry and exit sections to measure the bulk temperature of the nanofluid. The comparison of the two results is shown in Fig. 5. Lastly, the pressure drop between the inlet and outlet section at various Reynolds numbers was compared with the analytical solution. The comparison of the two is shown in Fig. 6.

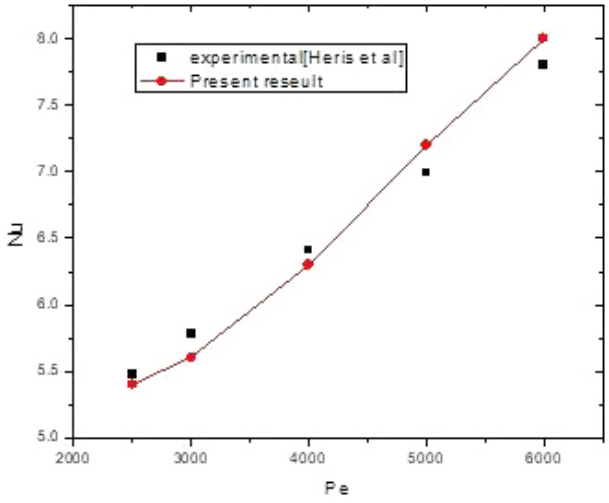

Figure 5: Comparison average Nusselt number against Peclet number with experimental data of Heris *et al.* [42].

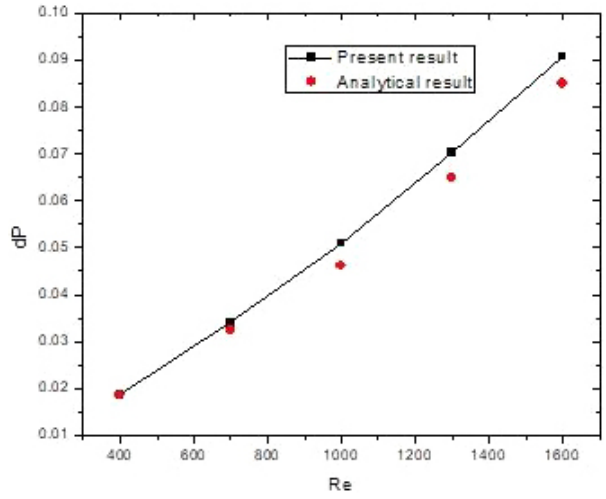

Figure 6: Comparison of pressure drop with analytical solution.

4 Results and discussion

This section deals with the results and discussion of the effects of Reynolds number ($300 \leq \mathrm{Re} \leq 1200$), nanoparticle concentration ($0\% \leq \varphi \leq 3\%$) and convergence index ($0 \leq n \leq 3$) on hydrodynamic and heat transfer performance of Al_2O_3/H_2O nanofluid flowing through novel Bessel-like converging pipes in laminar flow regime using the computational fluid dynamic approach and response surface methodology for the design of experiment.

4.1 Hydrodynamics

Figure 7 presents the velocity profile of Al_2O_3/H_2O nanofluid flowing through H0, H1, H2, and H3 at the Reynolds number of 300. The profiles showed

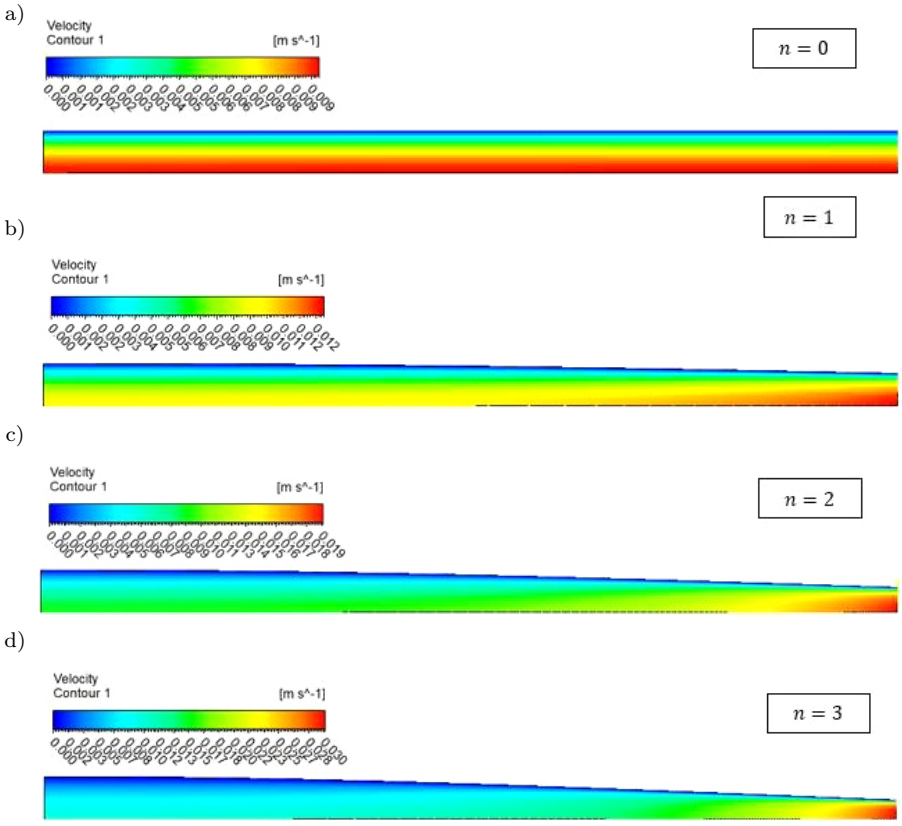

Figure 7: Variation of velocity profile for various pipe configuration at Reynolds number 300 and nanoparticle concentration of 2%: a) straight pipe, b)–d) converging pipe.

zero velocity at the wall, which is in agreement with no-slip boundary conditions imposed on the model. Also, it could be seen that the velocity profile in H0 is fully developed from the entry to exit plane. However, the velocity profiles in the converging pipes (H1, H2, and H3) changed along the axial distance.

To further confirmed this, the velocity profiles, $u_x(r)$, in H0, H1, H2, and H3 at the inlet, middle, and outlet sections are shown in Figs. 8a–d. The figures revealed that the $u_x(r)$ in the H0 is the same at the three locations and also satisfies the Poiseuille velocity profile expressed as $u_x = u_{in}\left[1 - \left(\frac{r}{R}\right)^2\right]$. This confirms that the flow is fully developed. However, the $u_x(r)$ in converging pipes (H0, H1, and H2) changed as the flow progress

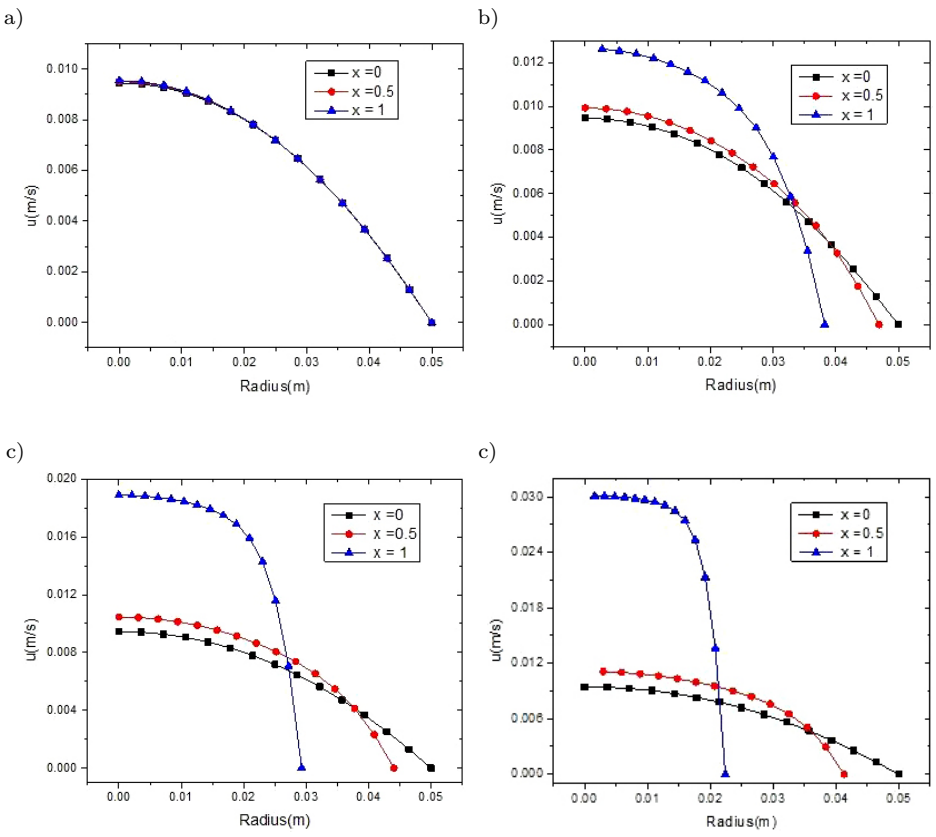

Figure 8: Variation of axial velocity in radial direction along the pipe length: a) $n = 0$, b) $n = 1$, c) $n = 2$, d) $n = 3$.

along the axial direction and did not satisfy the Poiseuille velocity profile at the middle and outlet planes. The change in $u_x(r)$ observed in converging pipes is attributed to a progressive decrease in cross-sectional area along the axial direction which leads to a progressive increase in nanofluid velocity.

Figures 9a and 9b show the local pressure drop, dP, distribution between the inlet and exit planes in H0 H1, H2, and H3 at Re = 300 and 900, respectively. The profiles reveal that dP in the converging pipes (H1, H2, and H3) has a parabolic behaviour in contrast to the linear curve obtained in the straight pipe (H0). This is in agreement with the work of Al-Sammarraie *et al.* [8]. The parabolic nature of dP in converging pipes is attributed to the progressive non-linear increase of local axial velocity of the nanofluid which leads to an increase in dP [36]. Figure 10 shows the variation of the pressure drop against the Reynolds number in all pipe configurations considered. The profiles reveal that an increase in convergence index enhances pressure drop. For instance, at the Reynolds number of 1200, dP in H0, H1, H2, and H3 is 0.1, 0.63, 2.3, and 7.33, respectively. Furthermore, it could be seen that an increase in Reynolds number enhances pressure drop. For instance, across the range of Reynolds number considered ($300 \leq \text{Re} \leq 1200$), the percentage increase in dP in H0, H1, H2 and H3 is 79.8%, 80.99%, 91.6% and 92.2% respectively. This result is expected as an increase in Reynolds number enhances velocity gradient (shear stress), which in turn leads to an increase in dP [43]. Figure 11 shows the influence of nanoparticle concentration on pressure drop. The graph shows that an increase in nanoparticle concentration enhances the pressure drop. For instance, across the range

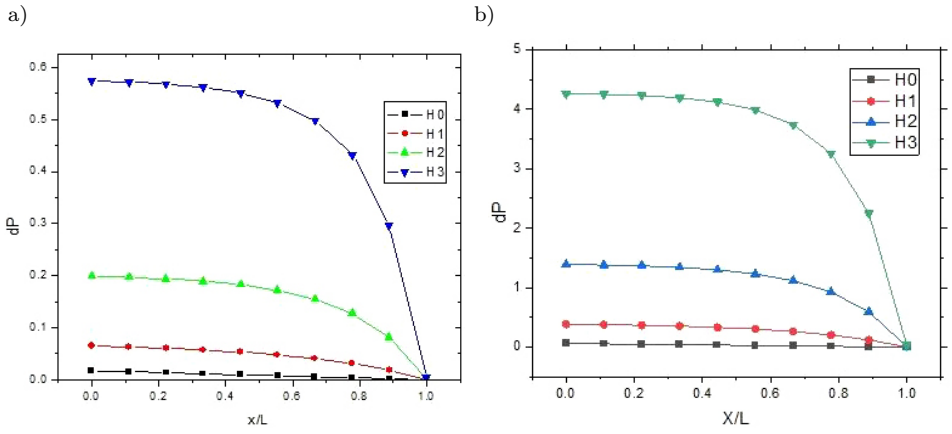

Figure 9: Variation of pressure drop along the pipe length: a) Re = 300, b) Re = 900.

of nanoparticle concentration ($0\% \leq \varphi \leq 3\%$) considered, at the Reynolds number of 600, the local pressure drop increases by 35.7% in all pipe configurations considered. This high increment in local pressure drop observed is attributed to the non-linear increase in viscosity of the nanofluid as the nanoparticle concentration increases as expressed in Eq. (11).

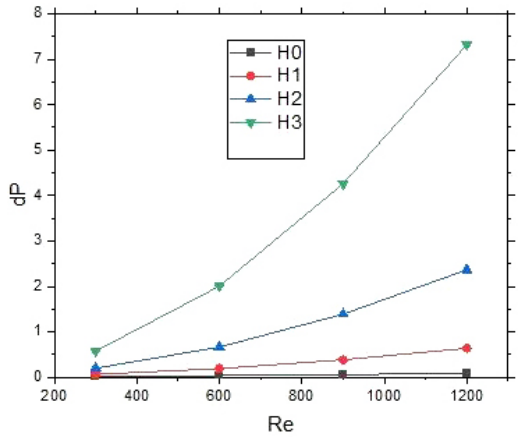

Figure 10: Variation of pressure drop against Reynolds number at nanoparticle volume fraction of 2%.

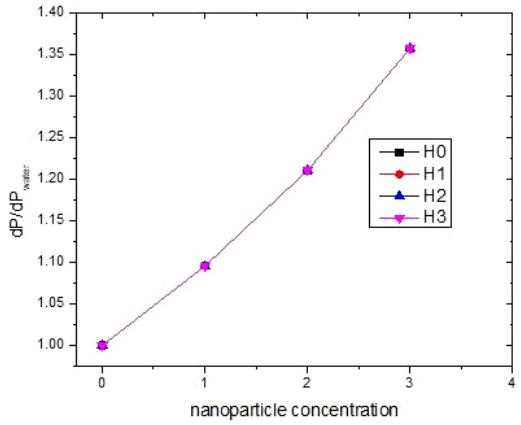

Figure 11: Variation of pressure drop against Reynolds number for various nanoparticle concentration in straight pipe at Re = 600.

Figures 12a and 12b show the variation of local friction factor, $C_f(x)$, along the axial direction in H0, H1, H2, and H3 at the Reynolds numbers 300 and 600. The profiles reveal that the local friction factor increases along

the axial direction of the converging pipes (H1, H2, and H3) in contrast to the constant value observed in the straight pipe (H0). The high value of $C_f(x)$ observed in converging pipes is attributed to high wall shear stress induced by an increase in convergence index. It should be noted that an increase in the converging index enhances the velocity gradient, which in turn raises the wall shear stress. Figure 13 shows the variation of the average friction factor, f, with the Reynolds number in all pipe configurations considered. The graph reveals that an increase in the convergence index enhances the average friction factor. For instance, the values of normalized

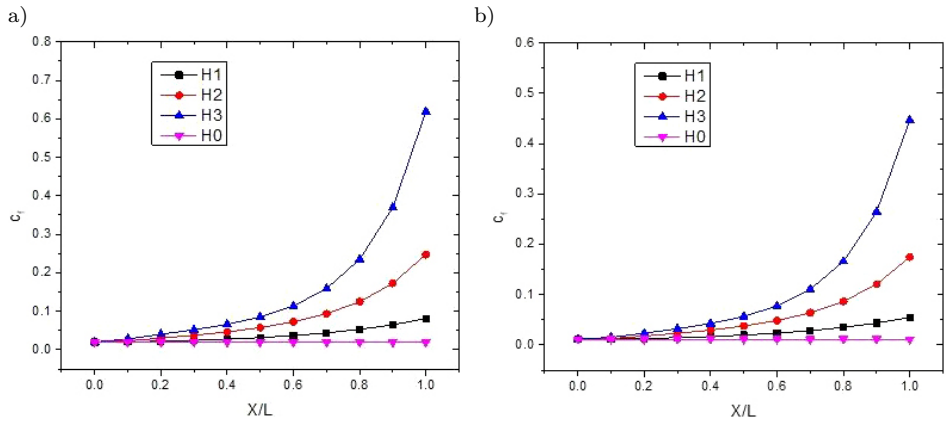

Figure 12: Variation of local friction coefficient: a) Re = 300, b) Re = 600.

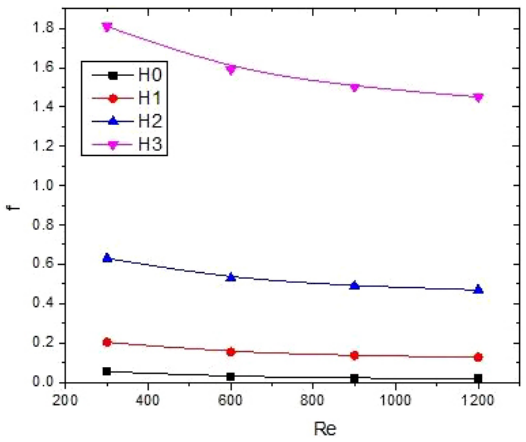

Figure 13: Variation of friction factor against Reynolds number for various pipe geometries.

friction factor (the ratio of f in converging pipes to corresponding value in the straight pipe) in H1, H2, and H3 at the Reynolds number of 900 are 6.43, 23.2, and 71.2, respectively.

4.2 Heat transfer

Figure 14 shows the temperature contours of Al_2O_3/H_2O nanofluid flowing through H0, H1, H2, and H3 at Reynolds number of 300. The contours reveal that the pipe wall has the maximum temperature which is in agreement with the boundary condition imposed $(q''_{\text{wall}} = 10^3)$. The profile also reveals that the thickness of the thermal boundary layer, δ_{th} grows progressively

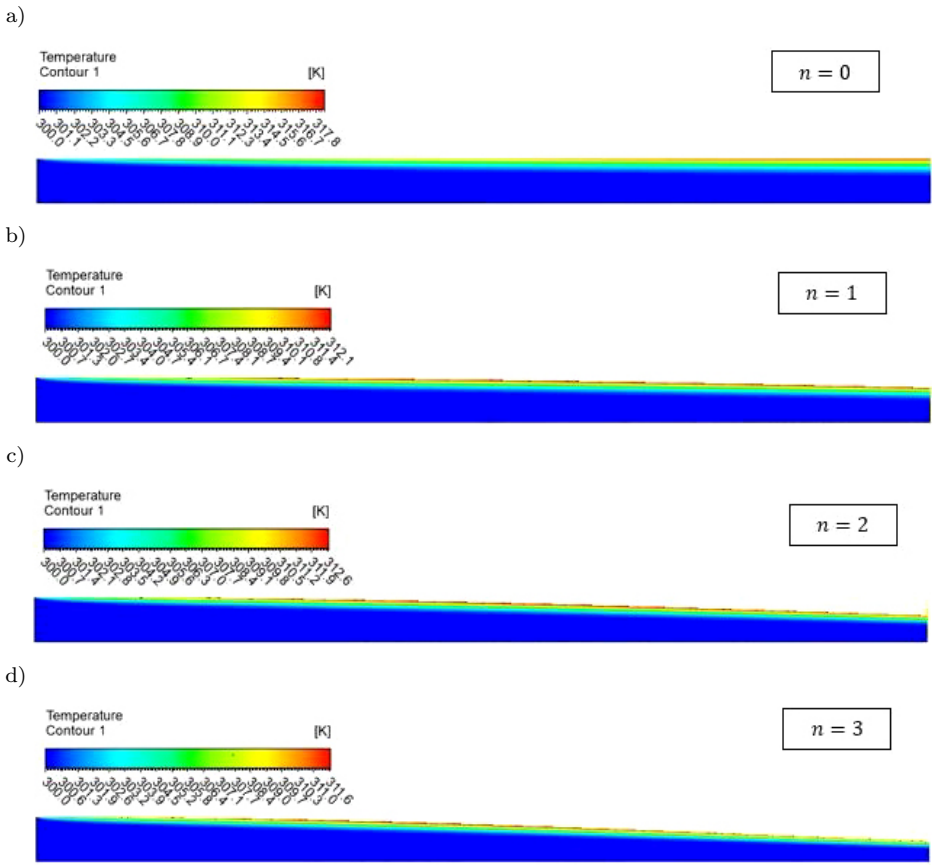

Figure 14: Variation of temperature profile for various pipe configuration at Reynolds number 300 and nanoparticle concentration of 2%: a) straight pipe, b)–d) converging pipe.

along the axial distance of the pipe. However, the growth rate decreases as the convergence index increases. The reduction observed is attributed to an increase in axial velocity due to progressive contraction of the cross-sectional area of the pipe along the axial direction. It should be noted that an increase in velocity diminishes thickness of the thermal boundary layer, as it has been shown that $\delta_{th} \propto \dfrac{\mathrm{Pr}^{-0.5}}{\sqrt{\mathrm{Re}}}$ [44].

Figures 15a and 15b show the distribution of pipe wall temperature, T_s at the Reynolds numbers 300 and 900, respectively. T_s of the converging pipes (H1, H2, and H3) increases from the entry plane to a certain point then begins to decrease toward the exit plane in contrast to the straight pipe (H0), in which T_s rises from the entry plane to the exit plane. This is in agreement with the work of Al-Sammarraie *et al.* [8]. Also, T_s decreases as the convergence index increases. The low value of T_s observed in converging pipes (H1, H2, and H3) is attributed to a high local axial velocity of the nanofluid which decreases δ_{th} and as a result, much heat is being transported from the surface of the pipe through the convection process. It should be emphasized here that the lower the thickness of the thermal boundary layer around a hot solid the higher the rate of convective heat transfers from it.

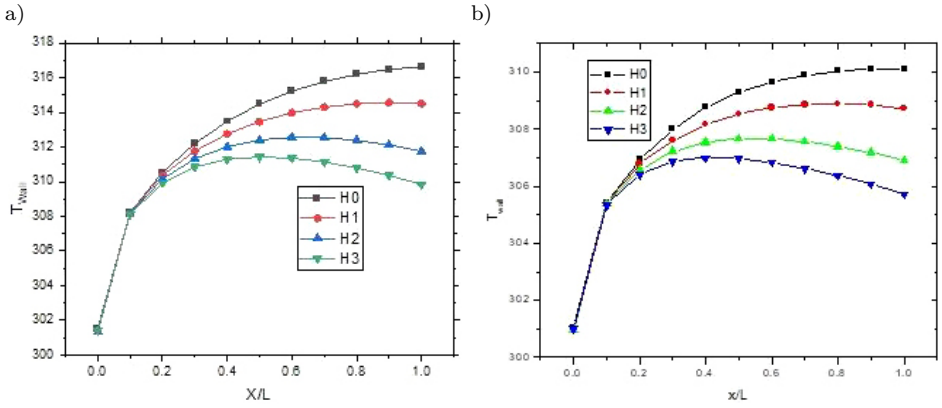

Figure 15: Graph of local wall temperature: a) Re = 300, b) Re = 900.

Figures 16a and 16b show the variation of the local Nusselt number, (Nu_x), along the pipe wall at the Reynolds numbers of 300 and 900, respectively. The profiles reveal that an increase in the converging index enhances convective heat transfer. The figure also shows that toward the exit plane, the local Nusselt number in H1, H2, and H3 exhibits an upward

trend in contrast to the downward trend obtained in H0. This result is attributed to the thickness of the thermal boundary layer which decreases as the convergence index increases.

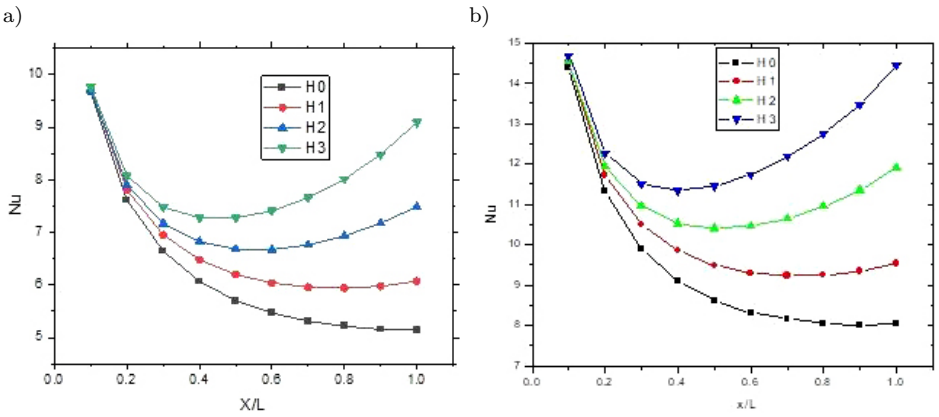

Figure 16: Graph of local Nusselt number: a) Re = 300, b) Re = 900.

Figure 17 shows the distribution of the average Nusselt number, Nu, against the Reynolds number in all pipe configurations considered. The profile reveals that an increment in convergence index enhances the Nusselt number. For instance, the values of the normalized average Nusselt number (the ratio of Nu in converging pipes to the corresponding value in the straight pipe) at the Reynolds number of 1200 in H1, H2, and H3 are

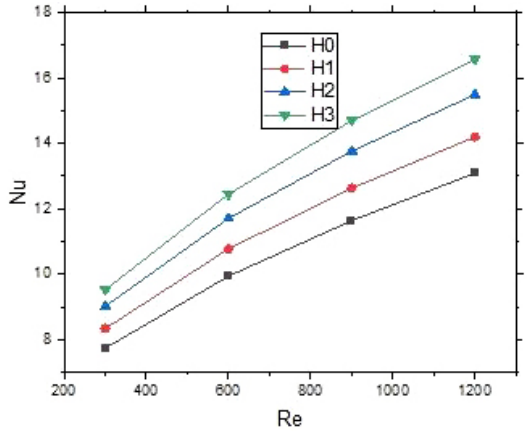

Figure 17: Graph of average Nusselt number against Reynolds number at nanoparticle concentration of 2%.

1.11, 1.25, and 1.37, respectively. The profile also shows that an increase in Reynolds number enhances average Nusselt number. For instance, at the Reynolds number of 300, the values of Nu in H0, H1, H2, and H3 are 7.8, 8.2, 9.0, and 9.6. Likewise, the values of the average Nusselt number at the Reynolds number of 1200 in H0, H1, H2, and H3 are 12.1, 13.0, 14.8, and 16.5, respectively.

Figure 18 shows the influence of nanoparticle concentration on the average Nusselt number. The profile reveals that an increase in nanoparticle concentration enhances Nusselt number. For instance, across the range of nanoparticle concentration ($0\% \leq \varphi \leq 3\%$) considered, the Nusselt number increases by 27%. The enhancement observed is due to an increase in thermal conductivity of the nanofluid which increases as the nanoparticle concentration increases [3].

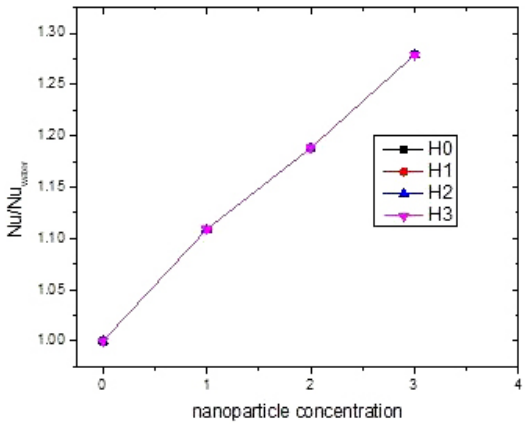

Figure 18: Variation of average Nusselt number against nanoparticle concentration at Reynolds number of 300.

Figure 19 shows the graph of geometry thermal performance criterion, $\mathrm{PEC}_{\mathrm{geo}}$, against the Reynolds number. The profile reveals that geometry thermal performance criterion decreases as the Reynolds number and convergence index increase. For example, the values of percentage reduction in $(\mathrm{PEC})_{\mathrm{geo}}$ in pipe H1, H2, and H3 across the range of Reynolds number considered are 19.8%, 23.6 % and 24.5%, respectively. The reduction in $\mathrm{PEC}_{\mathrm{geo}}$ observed is attributed to high local pressure drop accompanied by the enhancement in Nu. Thus, a Bessel-like converging pipe should be considered as a means of enhancing convective heat transfer at a low Reynolds number.

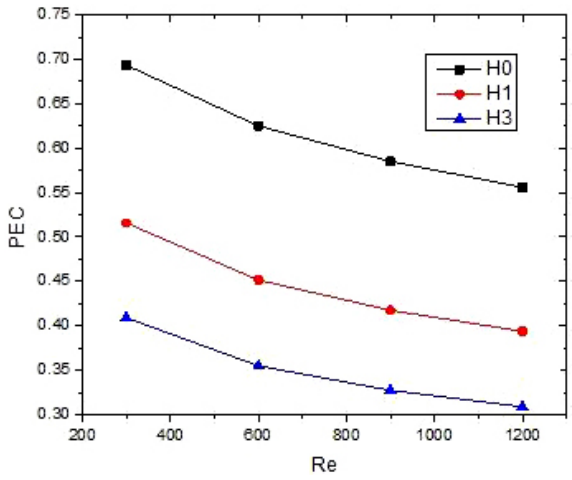

Figure 19: Variation of the geometry thermal performance criterion, $(PEC)_{geo}$, against Reynolds number in various converging pipes.

Figure 20 shows the variation of nanofluid performance evaluation criterion PEC_{nano} against nanoparticle concentration at the Reynolds number of 1200. The profile reveals that an increase in nanoparticle concentration enhances performance evaluation criterion. This implies that the usage of Al_2O_3/H_2O nanofluid as a heat transfer fluid is advantageous.

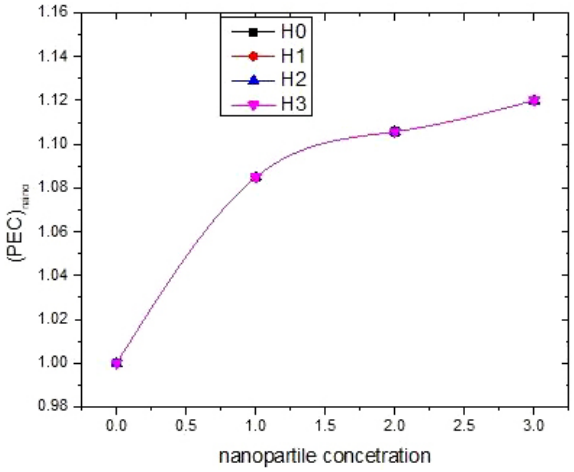

Figure 20: Variation of nanofluid performance evaluation criterion against nanoparticle concentration at Reynolds number of 300.

4.3 Response surface methodology

Table 5 shows the configurations of 3 independent variables (Reynolds number, convergence index, and nanoparticle concentration) and the corresponding values of the average Nusselt number of Al_2O_3/H_2O nanofluid in Bessel-like converging pipes. The quadratic function was used to fit the simulated data.

Table 5: The levels of the factors and the result of the Nusselt number.

Level	Re	n	φ	Nu × 10
1	600	1	1	1.11
2	1200	1	1	1.46
3	600	3	3	1.34
4	1200	3	1	1.71
5	600	1	3	1.16
6	1200	1	3	1.53
7	600	3	3	1.34
8	1200	3	3	1.79
9	600	2	2	1.24
10	1200	2	2	1.64
11	900	1	3	1.37
12	900	3	2	1.473
13	900	2	1	1.44
14	900	2	3	1.48
15	900	2	2	1.45
16	900	2	2	1.45
17	900	2	2	1.45
18	900	2	2	1.45
19	900	2	2	1.45
20	900	2	2	1.45

The result of the analysis of variance (ANOVA) is shown in Table 6. The coefficient of determination, R^2, is a statistical measure of how close the data are to the fitted regression line. The value of R^2 is 0.995 which is close to 1, this implies a good approximation. Also, the difference between the adjusted mean square, R^2_{adj}, and predicted mean square, R^2_{pre}, was 0.0085 which is less than 0.2 and, this shows that the model is suitable [45]. Note that R^2_{adj} represents the modified R^2 based on the number of

independent variables and R^2_{pre} measures the predictive capacity of the regression model. The null hypothesis (Reynolds number, convergence index and nanoparticle concentration did not have a significant influence on the Nusselt number) was rejected because the p-value of the ANOVA model is less than 0.05 [46]. Furthermore, Table 5 shows that the three input variables and some interaction between them are statistically significant (their p-values are less than 0.05) to the average Nusselt number of the Al_2O_3/H_2O nanofluid.

Table 6: Result of ANOVA for Nusselt number.

	Sum of square $\times 10$	Degree of freedom	Mean square $\times 10$	F-value $\times 10^3$	p-value
Model	4.94	6	0.82	0.430	<0.0001
Re	3.83	1	3.83	2.000	<0.0001
n	0.98	1	0.98	0.510	<0.0001
vol	0.10	1	0.103	0.050	<0.0001
Re $\times$ n	0.03	1	0.03	0.010	0.0021
n^2	0.06	1	0.06	0.030	0.0001
vol^2	0.02	1	0.02	0.008	0.0135
$n \times$ vol	0.03	13	0.02	–	<0.0001
Residual	0.03	7	0	–	–

$R^2 = 0.995$, $(R^2_{\text{pre}} - R^2) - (R^2_{\text{pre}} - R^2) = 0.0085$, adeq-precision = 81.766

The empirical model obtained is expressed as

$$\text{Nu}_{\text{ave}} = 14.46 + 2.0\text{Re} + 1.02n + 0.337\varphi + 0.193\text{Re} \times n - 0.482n^2 + 0.257\varphi^2 \,. \quad (24)$$

The value of the adeq-precision of the model was 81.77, since the value is greater than 4 it indicated the suitability of the model [47]. Furthermore, the accuracy of the model was ascertained by plotting the graph of normal probability against residual as shown in Fig. 21. The profile shows that most of the points follow a straight line which confirms the non-normality in the error terms [47]. Also, Fig. 22 shows the graph of predicted value against simulated data. The profile reveals that all data points fall on the regression line which confirms the accuracy of the model.

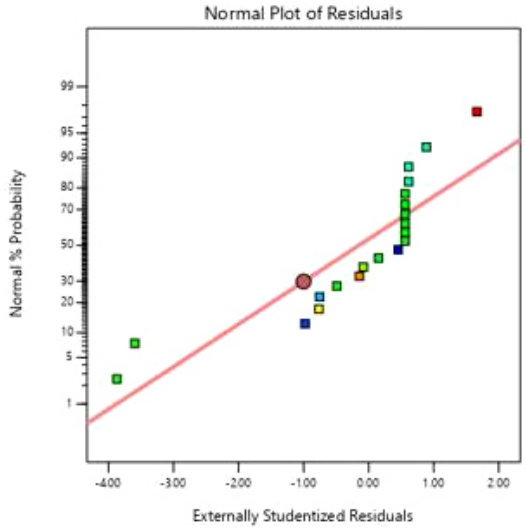

Figure 21: Graph of normal probability of average Nusselt number against residual.

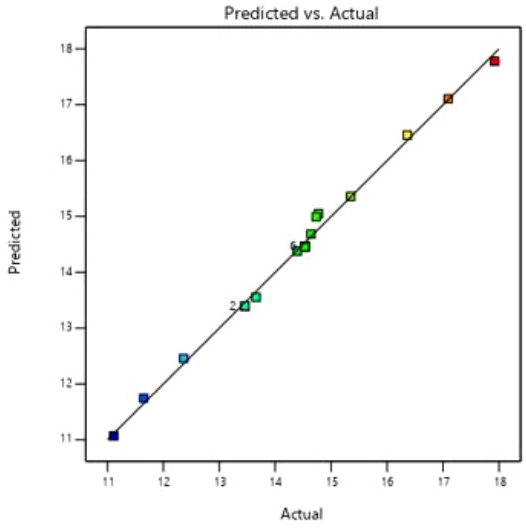

Figure 22: Graph of predicted value of Nusselt number against actual value.

4.4 Sensitivity analysis

Sensitivity analysis is the process of determining how a change in input parameters affects the output parameter. This can be achieved by taking the partial derivative of the output variable function with respect to input

variables. The positive value of the sensitivity connotes an increment in the input variable and corresponds to an increment in the output variable, while a negative value implies the opposite [48]. The partial derivative of Eq. (24) with respect to the three input parameters is expressed as:

$$\frac{\partial \mathrm{Nu}}{\partial \mathrm{Re}} = 2 + 0.193n\,, \tag{25}$$

$$\frac{\partial \mathrm{Nu}}{\partial n} = 1.2 + 0.192\mathrm{Re} - 0.964n\,, \tag{26}$$

$$\frac{\partial \mathrm{Nu}}{\partial \varphi} = 0.3369 + 0.512\varphi\,. \tag{27}$$

Table 7 reveals the result of sensitivity of the average Nusselt number to Reynolds number, nanoparticle concentration and convergence index at various configurations. The table reveals that the three input variables have positive sensitivity to the average Nusselt number in all configurations except nanoparticle concentration which has a negative sensitivity at configurations ($\mathrm{Re} = 0$, $n = 1$, $\varphi = -1$), In addition, among the three, the Reynolds number has the highest sensitivity of 2.192 which occurred at ($\mathrm{Re} = 0$, $n = 1$, $-1 \leq \varphi \leq 1$) followed by the convergent index 2.173 at ($\mathrm{Re} = 1$, $n = -1$, $\varphi = 0$) and lastly nanoparticle concentration 0.874 at ($-1 \leq \mathrm{Re} \leq 1$, $n = 0$, $\varphi = 1$).

Table 7: Result of sensitivity analysis of average Nusselt number.

Variable			Sensitivity		
Re	n	φ	$\frac{\partial \mathrm{Nu}}{\partial \mathrm{Re}}$	$\frac{\partial \mathrm{Nu}}{\partial n}$	$\frac{\partial \mathrm{Nu}}{\partial \varphi}$
–1	0	1	2	0.827	0.847
0	0	1	2	1.020	0.847
1	0	1	2	1.213	0.847
1	–1	0	1.808	2.173	0.337
1	0	0	2	1.213	0.337
1	1	0	2.192	0.253	0.337
0	1	–1	2.192	0.060	–0.173
0	1	0	2.192	0.060	0.337
0	1	1	2.192	0.060	0.847

5 Conclusion

The hydrodynamic and heat transfer performance of Al_2O_3/H_2O nanofluid flowing through a Bessel-like converging pipe has been investigated numerically using the computational fluid dynamics method. The effect of Reynolds number, convergence index, and nanoparticle concentration on hydrodynamic and heat transfer performance has been discussed in full detail. In addition, a new empirical correlation has been developed to estimate the average Nusselt number of Al_2O_3/H_2O nanofluid as a function of the aforementioned three variables. Lastly, a sensitivity analysis was carried out on the empirical model developed.

The results show that an increase in convergence index enhances the pressure drop and average Nusselt number. For instance, at the Reynolds number 1200 the values of pressure drop in H0, H1, H2 and H3, are 0.1, 0.63, 2.3, and 7.33, respectively. Likewise, the average Nusselt number assumes 12.1, 13.0, 14.8, and 16.5, respectively. Also, across the range of nanoparticle concentration considered ($0\% \leq \varphi \leq 3\%$), the average Nusselt number increases by 27%. In addition, the maximum values of the performance evaluation criterion (PEC) in H1, H2 and H3 are 0.7, 0.525, and 0.43, respectively, and decrease as the Reynolds number increases. Furthermore, across the range of Reynolds number considered ($300 \leq \mathrm{Re} \leq 1200$) the average Nusselt number increases by 55.1%, 58.5%, 64.4%, and 71.9% in H0, H1, H2, and H3, respectively. Finally, all three variables are statistically significant to the average Nusselt number.

Received 1 January 2021

References

[1] Kaood A., Abou-Deif T., Eltahan H., Yehia M.A., Khalil E.E.: *Numerical investigation of heat transfer and friction characteristics for turbulent flow in various corrugated tubes.* Mech. Eng. A.-J. Pow. **233**(2019), 4, 457–475.

[2] Kaood A., Hassan M.A.: *Thermo-hydraulic performance of nanofluids flow in various internally corrugated tubes.* Chem. Eng. Proces. – Process Intensif. **154**(2020), 108043.

[3] Owojori A.A., Olokuntoye B.A., Fadodun O.G.: *Numerical investigation of second law analysis of PGGNP/H_2O nanofluid in various converging pipes.* Int. Nano Lett., **11**(2021), 43–57.

[4] Khodabandeh E., Rozati S.A., Joshaghani M., Akbari O.A., Akbari S., Toghraie D.: *Thermal performance improvement in water nanofluid/GNP–SDBS*

in novel design of double-layer microchannel heat sink with sinusoidal cavities and rectangular ribs. J. Therm. Anal. Calorim. **136**(2019), 3, 1333–1345.

[5] Fadodun O.G., Amosun A.A., Salau A.O., Ogundeji J.A.: *Numerical investigation of thermal performance of singlewalled carbon nanotube nanofluid under turbulent flow conditions*. Eng. Rep. **1**(2019), 1–19, e12024.

[6] Sarkar M., Paramane S.B., Sharma A.: *Periodically fully developed heat and fluid flow characteristics in a furrowed wavy channel*. Heat Transfer Eng. **38**(2017), 2, 278–288.

[7] Fadodun O.G, Amosun A.A, Okoli N.L., Olaloye D.A, Ogundeji J.A., Durodola S.S.: *Numerical investigation of entropy production in $SWCNT/H_2O$ nanofluid flowing through inwardly corrugated tube in turbulent flow regime*. J. Therm. Anal. Calorim. **144**(2021), 4, 1451–1466.

[8] Al-Sammarraie A.T., Vafai K.: *Heat transfer augmentation through convergence angles in a pipe*. Numer. Heat Tr. A-Appl. **72**(2017), 3, 197–214.

[9] Al-Sammarraie A.T., Al-Jethelah M., Salimpour M.R., Vafai K.: *Nanofluids transport through a novel concave/convex convergent pipe*. Numer. Heat Tr. A-Appl. **75**(2019), 2, 91–109.

[10] Davood T., Omid A.A, Ali K., Ramin M.: *Numerical investigation of turbulent nanofluid flow and two-dimensional forced-convection heat transfer in a sinusoidal converging-diverging channel*. Heat Transf. Res. **50**(2019), 7, 671–695.

[11] Xie Y., Zheng L., Zhang D., Xie G.: *Entropy generation and heat transfer performances of Al2O3-water nanofluid transitional flow in rectangular channels with dimples and protrusions*. Entropy **18**(2016), 4, 148–160.

[12] Anvari A., Javaherdeh K., Emami-Meibodi M.: *Performance evaluation of a new Nano fluid through micro channels heat exchanger*. Chem. Engineer Trans. **71**(2018), 973–978.

[13] Salman S.D.: *Comparative study on heat transfer enhancement of nanofluids flow in ribs tube using CFD simulation*. Heat Transf. – Asian Res **48**(2019), 1, 148–163.

[14] Huminic G., Huminic A.: *A numerical approach on hybrid nanofluid behavior in laminar duct flow with various cross sections*. J. Therm. Anal. Calorim., **144**(2020), 5, 2097–2110.

[15] Pourfattah F.: *The effect of aspect ratios of rib on the heat transfer and laminar water/TiO2 nanofluid flow in a two-dimensional rectangular microchannel*. J. Mol. Liq. **236**(2017), 254–265.

[16] Khoshvaght-Aliabadi M.: *Influence of different design parameters and Al_2O_3–water nanofluid flow on heat transfer and flow characteristics of sinusoidal-corrugated channels*. Energ. Convers. Manage. **88**(2014), 96–105.

[17] Rashidi A.T., Akbarzadeh M., Karimi N., Masoodi R.: *Combined effects of nanofluid and transverse twisted-baffles on the flow structures heat transfer and irreversibilities inside a square duct*. J. Appl. Therm. Eng. **5**(2018), 7, 651–675.

[18] Manca O., Nardini S., Ricci D., Tamburrino S.: *Numerical investigation on mixed convection in triangular cross-section ducts with nanofluids*. Adv. Mech. Eng. **4**(2012), 1, 1–13.

[19] Ahmed M.A., Yusoff M.Z., Shuaib N.H., Ng K.C.: *A numerical study of laminar forced convection flow of Al_2O_3–water nanofluid in triangular-corrugated channel.* IOP C. Ser. Earth Env. **16**(2013), 1, 2149–2153.

[20] Aydar A.Y.: *Utilization of response surface methodology in optimization of extraction of plant materials.* In: Statistical Approaches with Emphasis on Design of Experiments Applied to Chemical Processes (V. Silva, Ed.). InTech, 2018, Chapt. 10, 157–169.

[21] Fadodun O.G, Salau A.O, Amosun A.A, Ibitoye F.I.: *Sensitivity analysis and evaluation of critical size of reactor using response surface methdodlogy.* Int. J. Emerg. Technol. **10**(2019), 4 184–190.

[22] Fadodun O.G, Amosun A.A; Salau A.O, Olaloye D.O, Ogundeji J.O, Ibitoye F.I, Balogun F.A.: *Numerical investigation and sensitivity analysis of turbulent heat transfer and pressure drop of Al_2O_3/H_2O nanofluid in straight pipe using response surface methodology.* Arch. Thermodyn. **41**(2020), 1, 3–30.

[23] Fadodun O.G, Olokuntoye B.A; Salau A.O, Amosun A.A.: *Numerical investigation and sensitivity analysis of entropy production in Al_2O_3/H_2O nanofluid in straight pipe using response surface methodology.* Arch. Thermodyn. **41**(2020), 2, 119–146.

[24] Shirvan K. M., Mamourian M., Mirzakhanlari S., Ellahi R.: *Two-phase simulation and sensitivity analysis of effective parameters on combined heat transfer and pressure drop in a solar heat exchanger filled with nanofluid by RSM.* J. Mol. Liq. **220**(2016), 888–901.

[25] Fadodun O.G, Amosun A.A., Okoli N. L. Olaloye D.O, Solomon S.D and Ogundeji J.A.: *Sensitivity analysis of entropy production in Al_2O_3/H_2O nanofluid through converging pipe.* J. Therm. Anal. Calorim. 143(2021), 1, 431–444.

[26] Chan J.S., Ghadimi A., Simon H., Metselaar, C., Lotfizadehdehkordi B.: *Optimization of temperature and velocity on heat transfer enhancement of nonaqueous alumina nanofluid.* J. Eng. Sci. Technol. **10**(2015) 85–101.

[27] Nookaraju B.C., Kurmarao P.S.V., Nagasarada S., Karthikeyan R., Vinay A.: *Optimization of process parameters of helical grooved heat pipe using response surface methodology.* Mater. Today: Proc. **5**(2018), 2, 5262–5271.

[28] Saha G., Paul M.C.: *Heat transfer and entropy generation of turbulent forced convection flow of nanofluids in a heated pipe.* Int. Commun. Heat Mass **61**(2015), 26–36.

[29] Kays W.M., Crawford M.E.: *Convection Heat and Mass Transfer* (2nd Edn.). McGraw Hill, New York 1980.

[30] Buongiorno J.: *Convective transport in nanofluids.* J. Heat Transf. **128**(2006), 3, 240–250.

[31] Xuan Y., Roetzel W.: *Conceptions for heat transfer correlation of nanofluids.* Int. J. Heat Mass Trans. **43**(2000), 19, 3701–3707.

[32] Corcione M.: *Empirical correlating equations for predicting the effective thermal conductivity and dynamic viscosity of nanofluids.* Energ. Convers. Manage. **52**(2011), 1, 789–793.

[33] Bird R.B., Stewart W.E., Lightfoot, E.N.: *Transport Phenomena* (2nd Edn.). Wiley, 2007.

[34] Churchill S.W.: *Friction factor equation spans all fluid-flow regime*. Chem. Eng. J. **84**(1997), 24, 91–92.

[35] Shah R. K., London A. L.: *Laminar Flow Forced Convection in Ducts: A Source Book for Compact Heat Exchanger Analytical Data*. Academic Press, 2014.

[36] Kourkah F.F., Mahd D.K., Mirzaee M.: *Optimization of double pipe heat exchanger with response surface methodology using nanofluid and twisted tape*. Fluid Mech. **3**(2017), 3, 20–26.

[37] Design-Expert 8.0.7, Stat-Ease Inc., Minneapolis 2012.

[38] Andreozzi A., Manca O., Nardini S., Ricci D.: *Forced convection enhancement in channels with transversal ribs and nanofluids*. Appl. Therm. Eng. **98**(2016), 1, 1044–1053.

[39] Nadila N.I., Lazim T.M., Mat S.: *Verification of heat transfer enhancement in tube with spiral corrugation*. AIP Conf. Proc. **2062**(2019), 1, 020032-1-6.

[40] Fluent 14.0 Theory Guide, Fluent Inc., Pittsburgh 2012.

[41] Wen D., Ding, Y.: *Experimental investigation into convective heat transfer of nanofluids at the entrance region under laminar flow conditions*. Int. J. Heat Mass Tran. **47**(2004), 24, 5181–5188.

[42] Heris S.Z., Etemad S.G., Esfahany M.N.: *Experimental investigation of oxide nanofluids laminar flow convective heat transfer*. Int. Commun. Heat Mass **33**(2006), 4, 529–535

[43] Mwesigye A., Meyer J.P.: *Optimal thermal and thermodynamic performance of a solar parabolic trough receiver with different nanofluids and at different concentration ratios*. Appl. Energ. **193**(2017), 393–413

[44] Vigdorovich I.: *Turbulent thermal boundary layer on a plate. Reynolds analogy and heat transfer law over the entire range of Prandtl numbers*. Fluid Dyn. **52**(2017), 1, 631–645.

[45] Carley K.M., Kamneva N.Y., Reminga J.: *Response surface methodology*. CASOS Techn. Rep. CMU-ISRI-04-136. Carnegie-Mellon Univ., School of Computer Science, Pittsburgh 2004.

[46] Richard B.: *Design Expert 7. Introduction*. Loughborough Univ. Mathematics Learning Support Centre. Loughborough 2007.

[47] Khuri A.I., Mukhopadhyay S.: *Response surface methodology*. WIREs Comp. Stat. **2**(2010), 2, 128–149.

[48] Griewank A., Walther A.: *Evaluating Derivatives: Principles and Techniques of Algorithmic Differentiation* (2nd Edn.). SIAM, Philadelphia 2008.